

Comparative Study of Subspace and Group-Sparsity Methods in 2D Localization for Bistatic Radar Systems

Pallabi Biswas^{1*}, Samarendra Nath Sur², and Rabindranath Bera³

^{1*}Department of Electronics and Communication Engineering, Sikkim Manipal Institute of Technology, Majhitar, Sikkim Manipal University, Gangtok, Sikkim, India

²Department of Computer Science and Engineering, Sikkim Manipal Institute of Technology, Majhitar, Sikkim Manipal University, Gangtok, Sikkim, India

³Department of Electronics and Communication Engineering, IIT Kalyani, West Bengal, India

Abstract: Conventional automotive radar systems typically operate in a monostatic configuration, wherein the transmitter and receiver are co-located. However, recent advancements have explored bistatic radar architectures, where the transmitter and receiver are spatially separated. This study investigates a highway scenario in which a searching vehicle leverages a roadside radar unit to detect targets in its surrounding environment. To estimate the Direction of Arrival (DOA) along with range and Doppler information, sparse signal representation techniques are employed. Specifically, subspace-based algorithms such as Multiple Signal Classification (MUSIC) and Estimation of Signal Parameters via Rotational Invariance Techniques (ESPRIT), along with a Group Sparsity (GS)-based method, are applied for two-dimensional localization and Doppler shift estimation in a bistatic radar setup. A comparative performance analysis is presented among the MUSIC, ESPRIT, and GS approaches. Simulation results using MATLAB demonstrate that the GS method significantly reduces estimation error and enhances the accuracy of both target localization and Doppler frequency evaluation compared to traditional subspace-based techniques.

Keywords: Bistatic Radar, Group-Sparsity method, MUSIC, ESPRIT.

1. Introduction

In advanced driver assistance systems (ADAS), radar sensors are widely preferred for their ability to detect the range, velocity, and direction of targets, as well as to process data effectively under adverse weather conditions. Automotive radars operating in the 24 GHz and 77 GHz frequency bands are commonly integrated into automated and semi-automated vehicles to scan and sense the surrounding environment, thereby enhancing driver safety and decision-making [1]. Traditionally, these radars operate in a monostatic configuration, where the transmitter and receiver are co-located within the same unit [2]. Conversely, bistatic radar systems feature spatially separated transmitter and receiver units, with an additional reference receiver used for signal demodulation [3], [4]. Bistatic radar offers several advantages over its monostatic counterpart, including enhanced stealth detection capabilities and greater flexibility in system deployment. In this work, a bistatic Frequency-Modulated Continuous Wave (FMCW) radar system is considered for automotive applications, wherein roadside sensors are utilized for the estimation of target range, direction of arrival (DOA), and Doppler shift.

Automotive radar signal processing is a complex and multi-stage procedure that involves the detection of a target's range and velocity, direction of arrival (DOA) estimation, and subsequent target localization and tracking [5], [6]. The receiver antenna captures multiple signal echoes reflected from targets positioned at various directions, often accompanied by noise and clutter. These unwanted components complicate accurate target detection and localization. To ensure effective beamforming and to suppress interference, accurate DOA estimation of the desired

target signals is essential [7]. At the receiver, maximizing the signal-to-noise ratio (SNR) is crucial for mitigating the impact of interference and clutter, thereby enhancing the reliability and precision of the radar system.

DOA evaluation techniques can be classified under beamforming approaches, Maximum Likelihood Estimator and Subspace-based methods. The methods based on signal subspace models, like Multiple Signal Classification (MUSIC) and Estimation of Signal Parameters via Rotational Invariance Technique (ESPRIT), decompose the received signals into signal subspace and noise subspace and provide better resolution for the target [8]. MUSIC algorithm [9] depends on eigenvalue analysis of the signal covariance matrix to separate the signal subspace and noise subspace. Then search is conducted over all possible angles of arrival, and the angles are chosen that minimize the noise subspace. In place of angles, MUSIC can also be used to measure Doppler shifts. ESPRIT is based on the rotational invariance property of the signal subarrays to solve for DOAs, making it computationally faster than MUSIC and more efficient. The ESPRIT algorithm can be used in fast-time and slow-time arrays to estimate range and velocity. For simultaneous estimation of the range and the angle, a 2-dimensional MUSIC algorithm applied on FMCW MIMO Radar signal processing in distributed form has been proposed in [10]. Every Radar applies 2-dimensional MUSIC with its specific received signal and then sends its specific values of the cost function for the particular Radar image section. Then, the data fusion centre can evaluate the range and the direction of the targets jointly from the total cost function. For 2-dimensional DOA measurement in bistatic Radar, another method called reduced-dimension MUSIC can be used [11], where a 4-dimensional function of spatial spectrum is modified into a 2-dimensional search grid to reduce the complexities of computation and to improve performance. In [12], a Power Estimation MUSIC (PE-MUSIC) algorithm is proposed for solving the uncertainty of sparse array MIMO Radar for uncorrelated Radar sources. Initially, MUSIC is used to obtain the DOA of all real and false targets, then by applying Davidon–Fletcher–Powell (DFP) algorithm, power values of all the targets are calculated. The power values of false targets tend to zero and are hence eliminated, leading to reduced uncertainty. A 2-dimensional unitary ESPRIT-based algorithm for range-Doppler estimation in FMCW Radar has been provided in [13]. Here, a 1-dimensional intermediate frequency signal is modified to a 2-dimensional virtual array signal, which is reconstructed into a complex-value matrix. Then, the eigenvalue decomposition of this matrix results in the evaluation of the range and Doppler parameters of the multiple targets. In [14], for bistatic MIMO Radar having sparse linear arrays, a Reduced Dimension ESPRIT-MUSIC has been suggested for the target angle estimation, which reduces computational complexities. In [15], the coupled C-ESPRIT-based method for azimuth and location angle evaluation uses a minimum variance technique with a conjugate rotation matrix for processing information from every array element without taking them into groups. In case of a sparsity-based target scenario, the distributed DOA method can be applied for the estimation of sparse vectors [16]. In [17], a MIMO Radar architecture with non-uniform sparse arrays used for both transmitter and receiver is considered for high resolution DOA estimation with a single snapshot, with the help of the mutual coupling method. The transmitter and receiver antennas are separated into dual sub-arrays to obtain 2 sets of MIMO radars with sparse uniform virtual arrays. After spatial smoothing is applied, the virtual arrays can be used for DOA estimation. For angle and Doppler estimation in MIMO Radar, another signal processing technique called Group Sparsity (GS) is used, which considers that signals are sparse in structured groups like in range-Doppler bins [18]. The GS method is applied for the detection of multiple targets that have shared characteristics, like in range-Doppler bins and angles. Similarly, in [19], the estimation of the difference in Doppler is formulated as a GS-based reconstruction problem, where the search grid is shortened to one-fourth of the actual search grid for a multipath scenario. This helps to reduce

the computation cost and improves the performance. A signal processing method for DOA measurement based on Compressive Sensing (CS) theory is presented, which provides good resolution and accuracy while allowing an improved degree of design [20]. This algorithm can utilize configurations of sparse antennas with a smaller number of transmitter and receiver channels and a larger effective antenna aperture.

In this study, a bistatic roadside radar scenario is considered, wherein the radar unit transmits waveforms that are subsequently utilized by a searching vehicle to detect a target vehicle. A sparse representation of the bistatic radar signal is formulated to facilitate the estimation of two-dimensional target localization—comprising both range and DOA along with the Doppler shift of the target. By modeling the raw radar data using a sparse framework, the geometrical configuration of the bistatic system is reformulated such that the source vectors possess a generalized support set. This structural adaptation enables the effective application of the GS-based method. In parallel, classical subspace-based algorithms, namely MUSIC and ESPRIT, are also employed for estimating range, DOA, and Doppler. A comparative performance evaluation of these three techniques—GS, MUSIC, and ESPRIT—is conducted through computer simulations to assess their relative accuracies and robustness in bistatic automotive radar applications.

The contributions of this paper include:

- i. This paper presents a performance analysis of MUSIC, ESPRIT, and Group Sparsity (GS) methods for target localization and Doppler estimation in a bistatic radar scenario. The algorithms are compared based on their estimation error levels. With a limited number of sensors, the GS method—using a sparse matrix representation—shows greater resilience to signal variations and noise, offering improved DOA estimation over MUSIC and ESPRIT. Additionally, larger data matrices enhance the performance of the GS method by reducing estimation errors and providing a more accurate system representation.
- ii. An analysis of location and Doppler estimation using the GS technique with varying numbers of antennas is presented, highlighting its relevance to MIMO radar design. Increasing the number of antenna elements results in narrower beamwidths, thereby enhancing angular resolution and improving the ability to distinguish closely spaced targets.
- iii. Radar Cross Section (RCS) quantifies the strength of the backscattered signal from a target and depends on factors such as target range, signal power, operating wavelength, and aspect angle [21]. The performance of the GS-based method is evaluated by analyzing the estimation errors in location and Doppler parameters under varying RCS conditions.

The rest of this paper is categorized as follows: in section 2, a brief analysis of the FMCW bistatic Radar used as a sensor situated on the roadside is provided. In section 3, algorithms for location and Doppler measurement of the target have been explained, which include the MUSIC, the ESPRIT and the Group-sparsity based algorithm. Section 3 contains the simulation results and performance analysis of these algorithms. Finally, the conclusion is drawn in section 4.

2. Overview of FMCW Bistatic Radar

According to figure 1 shown below, it is assumed that a searching vehicle at R_x is using the signals transmitted from the roadside Radar at T_x to locate the target vehicle at T_g . The vehicle in searching mode is assumed to be proceeding towards the Radar on the roadside, and the target vehicle is assumed to be receding from it. The transmitted signal is a frame of M number of narrowband FMCW pulses, having T as pulse repetition interval and T_c as duration of pulse transmission [22], [23]. The advantage of using FMCW Radar is that the velocity and the range can be determined

simultaneously with high range resolution and low Probability of Interception (LPI) [24].

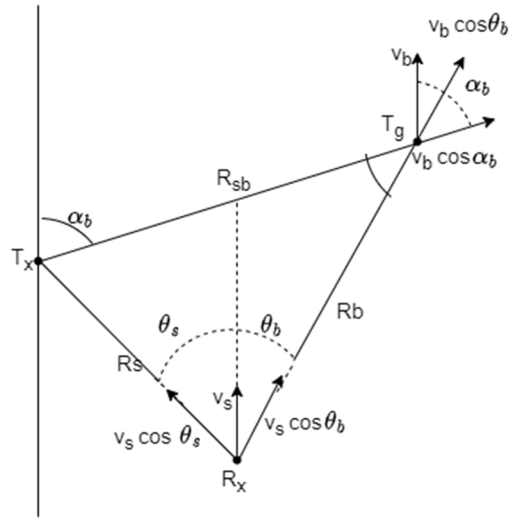


Figure 1. Figure Label.

A single chirp signal is represented as,

$$s_0(t) = \begin{cases} e^{[j2\pi(f_0t+0.5\mu t^2)]} & t \in [0, T_c] \\ 0 & otherwise \end{cases} \quad (1)$$

in which, $\mu = \frac{B}{T_c}$ is assumed as the rate of modulation with B as the bandwidth of modulation, f_0 as initial frequency and t as continuous time. This continuous time is classified into fast time (t_f) and slow time (t_s). Fast time is the time duration within a pulse, and the time period between pulses is defined as slow time. So, t is written as,

$$t = t_f + t_s = t_f + m_c T \quad t_f \in [0, T_c] \quad (2)$$

in which ($m_c = 0, 1, \dots, M_c - 1$) is taken as the chirp index. Considering a periodic transmit signal, a sequence of M chirps can be presented as,

$$s(t) = s(t_f + m_c T) = s_0(t_f) \quad (3)$$

It is assumed that the Radar on the roadside is static and the vehicles are in motion with a steady velocity, and their direction is forward in a way that the vehicle operating in searching mode is moving towards the Radar with a velocity v_s and the vehicle assumed as a target is moving away from it, having a velocity of v_b . Here, ‘s’ is used for parameters belonging to the direct path from the roadside Radar and ‘b’ is used for parameters belonging to the multipath from the b^{th} target vehicle. The Doppler on the signal of the direct path present due to the mobility of the searching vehicle is observed to be

$$V_s = -v_s \cos(\theta_s) \quad (4)$$

in which, θ_s is taken as the DOA of the Radar on the roadside. Likewise, the Doppler estimated on every path of the multi-path signal is observed to be,

$$V_b = v_b \cos(\alpha_b) + (v_b - v_s) \cos \theta_b, \quad (5)$$

$$\alpha_b = \arcsin\left(\frac{R_s}{\hat{R}_b - R_b} \sin(|\theta_s - \theta_b|)\right) + \theta_b \quad (6)$$

in which, R_s is the range distance between the Radar on the roadside and the vehicle operating in searching mode, and the location of the Radar is known. R_b is the range distance between the vehicle taken as the target and the vehicle operating in searching mode. ($\hat{R}_b = R_b + R_{sb}$) with R_{sb} as the range distance between the Radar on the roadside and the target vehicle and θ_b is the DOA of the vehicle assumed as the target. It is assumed that the searching vehicle has L number of antenna units forming a uniform linear array (ULA),

having spacing 'd' in-between the units. So, the mathematical model for the direct-path signal obtained at the vehicle working in searching mode corresponding to the Radar is,

$$r_s(l, m, t_f) = A_s s \left(t - \tau_s(m, t_f) \right) e^{j2\pi\varphi_s(l)}, \quad (7)$$

$$\text{And } \tau_s(m, t_f) = \frac{R_s}{c} + \frac{V_s}{c} (t_f + mT) \quad (8)$$

in where, τ_s is the delay in time, the delay in phase related to the first antenna unit, is ($\varphi_s(l) = \frac{f_0 d \sin \theta_s}{c} l$), and c is the velocity of light. The amplitude of the received signal of the direct path

$$A_s = \sqrt{\frac{P_t G_t G_r c^2}{(4\pi)^2 f_0^2 R_s^2}} \quad (9)$$

in where, G_r is the receiver gain. Likewise, the mathematical model for one multi-path signal obtained at the vehicle working in searching mode corresponding to the target vehicle 'b' is,

$$r_b(l, m, t_f) = A_b s \left(t - \tau_b(m, t_f) \right) e^{j2\pi\varphi_b(l)}, \quad (10)$$

$$\text{And } \tau_b(m, t_f) = \frac{\hat{R}_b}{c} + \frac{V_b}{c} (t_f + mT) \quad (11)$$

in where, τ_b is the delay in time, the delay in phase related to the first antenna unit, is ($\varphi_b(l) = \frac{f_0 d \sin \theta_b}{c} l$), and σ is the Radar Cross Section (RCS). The amplitude of the received signal of the multi-path

$$A_b = \sqrt{\frac{P_t G_t G_r \sigma c^2}{(4\pi)^3 f_0^2 R_b^2 R_{sb}^2}} \quad (12)$$

Thus, the received signal is a combination of both paths. The RCS value is obtained as,

$$\sigma = \frac{(4\pi)^3 f_0^2 R_b^2 R_{sb}^2}{P_t G_t G_r c^2 (A_b)^2} \quad (13)$$

To obtain the embedded data, cross-correlation is done of this signal with a signal similar to $s_0(t)$. For B number of targets, the signal with the intermediate frequency (IF) is given as,

$$y(l, m, t_f) = \sum_{b=1}^B r_b(l, m, t_f) s_0(t_f)^* + w(l, m, t_f), \quad (14)$$

in this, w is taken as the additive white Gaussian noise (AWGN). Then, the de-chirped signal is sampled at a rate of f_s , so that the sampling index is ($n = 0, 1, \dots, N-1$) where, the fast-time samples are given as $N = f_s T_c$. Finally, after mathematical calculations, the de-chirped signal is expressed in terms of l , fast time index n , and slow time index m ,

$$y[l, m, n] = \sum_{b=1}^B q_b \exp \left[-j2\pi \left(\frac{\mu \hat{R}_b}{c} \frac{n}{f_s} + \frac{f_0 V_b}{c} mT + \frac{f_0 d \sin \theta_b}{c} l \right) \right] + w[l, m, n] \quad (15)$$

in where, $q_b = A_b e^{-j2\pi(\frac{f_0 \hat{R}_b}{c})}$

Considering the Nyquist theorem, the maximum detectable multi-path range can be obtained as,

$$R_{max} = \frac{c f_s}{\mu} \quad (16)$$

The raw data of $y[l, m, n]$ can be presented in tensor form $Y \in \mathcal{C}^{L \times M \times N}$, so that,

$$Y = \sum_{b=1}^B q_b (a_b \circ v_b \circ r_b) + W \quad (17)$$

in where, $W \in \mathcal{C}^{L \times M \times N}$ is AWGN.

A ($L \times 1$) column vector, $a_b = [1, e^{-j2\pi(\frac{f_0 d \sin \theta_b}{c})(1)}, \dots, e^{-j2\pi(\frac{f_0 d \sin \theta_b}{c})(L-1)}]^T$

A ($M \times 1$) column vector, $v_b = [1, e^{-j2\pi(\frac{f_0 V_b}{c})(1)T}, \dots, e^{-j2\pi(\frac{f_0 V_b}{c})(M-1)T}]^T$

$$A \text{ (N*1) column vector, } r_b = [1, e^{-j2\pi\left(\frac{\mu\hat{R}_b}{c} \frac{1}{f_s}\right)}, \dots, e^{-j2\pi\left(\frac{\mu\hat{R}_b}{c} \frac{N-1}{f_s}\right)}]T \quad (18)$$

Considering that the parameters of the searching vehicle (R_s, θ_s). Then \hat{R}_b can be presented as,

$$\hat{R}_b = \sqrt{R_b^2 + R_s^2 - 2R_bR_s \cos(\theta_s - \theta_b)} + R_b \quad (19)$$

Then, the antenna units and the domains of fast-time are assembled against those of the slow-time. The tensor Y can be modified in the format of a matrix, $Y \in C^{LN \times M}$, in a way, $Y = \sum_{b=1}^B q_b (p_b v_b^T) + W$ (20)

in where, $p_b = (r_b \times a_b)$ and $W \in C^{LN \times M}$ is AWGN.

Lastly, Y can be presented as,

$$Y = PXV^T + W \quad (21)$$

in where, $P \in C^{LN \times B}$ consists of range-DOA data, $V \in C^{M \times B}$ consists of the Doppler data, and $X \in C^{B \times B}$ consists of the complex amplitude.

For representation of bistatic localisation evaluation in sparse format, a 2-dimensional polar grid consisting of size G_p is assumed to obtain the range and the DOA (R_{gp}, θ_{gp}) and evaluate (R_b, θ_b), with ($g_p = 1, 2, \dots, G_p$) presents the g_p th index of the grid. Next, a steering matrix containing values from range-DOA, $P_g \in C^{LN \times G_p}$ is created with the g_p -th column $P_{gp} = (\hat{r}_{gp} \times a_{gp})$, with

$$a_{gp} = [1, e^{-j2\pi\left(\frac{f_0 d \sin \theta_{gp}}{c}\right)(1)}, \dots, e^{-j2\pi\left(\frac{f_0 d \sin \theta_{gp}}{c}\right)(L-1)}]T \quad (22)$$

$$\text{and, } \hat{r}_{gp} = \begin{bmatrix} e^{-j2\pi\left(\frac{\mu\sqrt{R_{gp}^2 + R_s^2 - 2R_{gp}R_s \cos(\theta_s - \theta_{gp})} + R_{gp}}{c} \frac{1}{f_s}\right)} \\ e^{-j2\pi\left(\frac{\mu\sqrt{R_{gp}^2 + R_s^2 - 2R_{gp}R_s \cos(\theta_s - \theta_{gp})} + R_{gp}}{c} \frac{N-1}{f_s}\right)} \end{bmatrix} \quad (23)$$

$$Z^P = P_g X_g^P + W \quad (24)$$

In this, $X_g^P \in C^{G_p \times M}$ is defined as the sparse matrix of data, where the m^{th} column has B non-zero values related to complex coefficients of the targets.

For a representation of bistatic Doppler evaluation in sparse format, the Doppler grid consisting of size G_d is assumed to obtain the velocity (V_{gd}) and evaluate (V_b), with ($g_d = 1, 2, \dots, G_d$) presents the g_d th index of the grid. Next, a Doppler steering matrix $V_g \in C^{M \times G_d}$ is created with the V_{gd} in V, so that,

$$V_{gd} \in [V_{min}, V_{max}]$$

in where,

$$V_{min} = \min \{v_{min} \cos(\alpha_{g_{ij}}) + (v_{min} - v_s) \cos(\theta_{g_{ij}})\} \quad (25)$$

$$V_{max} = \max \{v_{max} \cos(\alpha_{g_{ij}}) + (v_{max} - v_s) \cos(\theta_{g_{ij}})\} \quad (26)$$

$$\alpha_{g_{ij}} = \arcsin \left(\frac{R_s \sin(|\theta_s - \theta_{g_{ij}}|)}{\sqrt{R_{g_{ij}}^2 + R_s^2 - 2R_{g_{ij}}R_s \cos(\theta_s - \theta_{g_{ij}})}} \right) + \theta_{g_{ij}} \quad \text{for all } g_{ij} \quad (27)$$

V_{min} = minimum value of the probable forward velocity of the vehicle taken as the target,

V_{max} = maximum value of the probable forward velocity of the vehicle taken as the target.

$$\text{Then, } Z^D = V_g X_g^D + W^T \quad (28)$$

with, $X_g^D \in C^{G_d \times LN}$, is defined as the sparse matrix of data, where the ln^{th} column has B non-zero values related to complex coefficients of targets.

3. Location and Doppler estimation algorithms

A roadside Radar system transmits a sequence of chirp signals, which is used by a searching vehicle to detect a target vehicle. Signals reflected from the target vehicle and clutter are a combination of various Radar echoes along with additive noise. This noise is reduced, and detection of the echoes obtained from different objects that are distinguishable in the domains of the range, the Doppler and the DOA, is done.

3.1. MUSIC algorithm:

In this subspace-based technique, the covariance matrix is disintegrated into both signal subspace and noise subspace. The steering vectors are perpendicular to the noise, and the required direction is obtained from the peak value in the spectrum of spatial power.

Algorithm 1: The procedure for the MUSIC method can be presented as [25]:

Considering the signal models as presented in equations 14 and 24, the steering matrix is presented by, P_g . The covariance matrix is presented as,

$$R_{cm} = P_g R_s (P_g)^H + \sigma^2 I \quad (29)$$

in where, R_s is the covariance matrix of the source signal, I is the identity matrix, H denotes the Hermitian response, and σ^2 is the variance of the sensor noise vector. The R_{cm} matrix can be disintegrated into matrices of eigenvectors and eigenvalues. The MUSIC algorithm's spatial spectrum is given as:

$$P_{Music} = 1 / [(P_g)^H U_N U_N^H P_g] \quad (30)$$

with U_N as the subspace of noise containing the eigenvectors relative to the eigenvalues obtained by eigen disintegration of R_{cm} .

3.2. ESPRIT algorithm:

This algorithm is computationally less complex than MUSIC as it does not consider all direction vectors. The subspace of incident signals is extended by two responses that are displaced from each other by a known vector, and from these, the DOA can be evaluated.

Algorithm 2: The procedure for the ESPRIT method can be presented as [25]:

- Considering the de-chirped signal model as shown in equation 24, in where, P_g is a range-DOA steering matrix, $X_g^P \in C^{G_p \times M}$ is defined as a sparse matrix of data and W is AWGN.
- The covariance matrix is created by collecting received signal data over time. The eigenvalue disintegration of this covariance matrix is done to get the signal subspace and noise subspace. Then the steering matrix P_g is considered.
- Using the rotational invariance characteristic of the subspace of the signal, the rotation matrix is calculated. Finally, DOA is estimated from the eigenvalues of this matrix.

3.3 Group-Sparsity method:

In this algorithm, the structured sparsity patterns of the received signals are studied for the detection of the target's location and DOA. It is considered that the source vectors have a common support set (e.g. range-Doppler bins).

Algorithm 3: The procedure for the ESPRIT method can be presented as:

- The raw Radar data is stored as shown in equation 20.
- A rectangular-shaped search grid is generated having length G_p , and the Cartesian location coordinates are changed to polar coordinates.
- Then, the range-DOA steering matrix is created, and the value of X_g^P is evaluated.
- A search for the peak is conducted to obtain the coordinates.
- Transpose of raw Radar data is obtained.
- By using proper values of v_{min} and v_{max} , and v_s and all G_p values, V_{min} and V_{max} are calculated.
- A Doppler search grid is generated having size G_d .

- h) Then the Doppler steering matrix V_g is created, with its g_d -th column corresponding to V_{gd} . Then the value of X_g^D is evaluated.
- i) A search for the peak is conducted to obtain the Doppler values.
- j) Using these evaluated coordinates, the values of R_b and θ_b are estimated. Finally, with these values, v_b is obtained.
- k) This $(x, y)_b$ and v_b values are calculated for all the B targets.

4. Performance analysis

Results are obtained from computer simulations using MATLAB to analyse the performances of the MUSIC, ESPRIT and GS algorithms for estimation of the location and the Doppler of a particular target vehicle, under varying levels of noise. The Radar parameters are provided in Table 1.

Table 1. The parameters of the Radar for the simulation process

Parameters	Value
Centre frequency	77 GHz
Chirp bandwidth	150 MHz
Sampling frequency	5 MHz
Modulation period	30 us
Pulse repetition frequency	35 us
No. of chirps	128

A single target vehicle is considered, and different algorithms are used for estimation of its location and Doppler. For the GS method, different tests are conducted to observe the result of the increment of data size on the working capability of the algorithm. This is done by changing the quantity of processed columns Q from the signal matrix, such as $Q = 1, 4, 8$, each test conducted with 50 iterations. In every iteration, a different noise signal is generated, and the Cartesian coordinates of the target's position and Doppler parameter are obtained from a consistent distribution limited by two adjoining grid points from the relative search grids. The performance is evaluated by the Root Mean Square Error (RMSE) of estimation versus the increasing levels of Signal to Noise Ratio (SNR). The RMSE measures the average difference between the estimated value and the actual value, thus indicating the accuracy of the algorithm. The MUSIC and ESPRIT algorithms were applied with 8 columns, which are processed (Q) from the matrix of signal values, for the capability to use the exact search grid as used by the GS method.

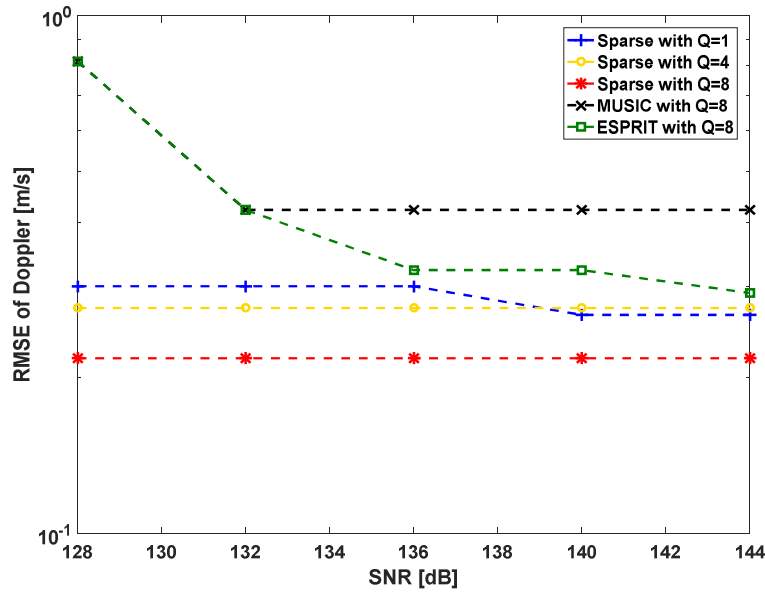


Figure 2. A comparative analysis of RMSE of Doppler v/s SNR for 1 target obtained with the Group-sparsity method, the MUSIC and the ESPRIT.

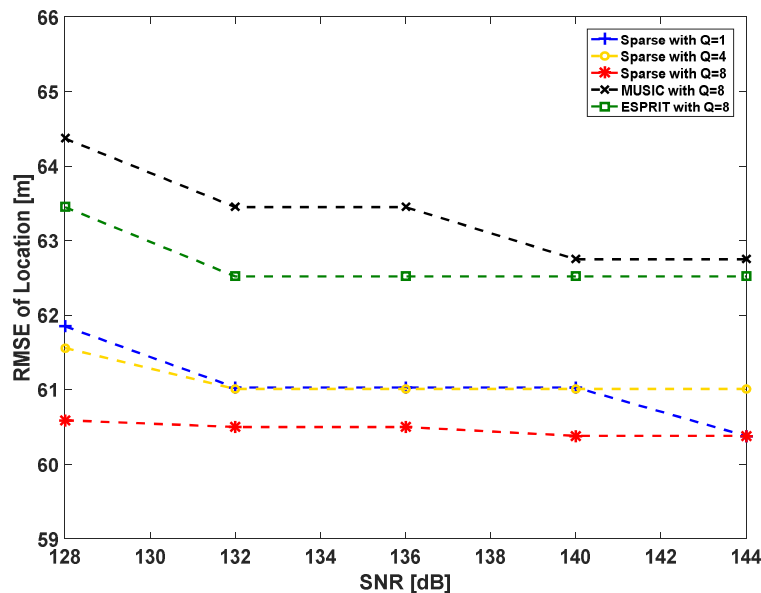


Figure 3. A comparative analysis of RMSE of location v/s SNR for 1 target obtained with the Group-sparsity method, the MUSIC and the ESPRIT.

As observed from figure 2, the RMSE of the Doppler value is highest for the MUSIC and the ESPRIT algorithms and lowest for the GS-based method, specifically for $Q = 8$, for increasing values of the SNR. For example, at the SNR value of 136dB, the RMSE of Doppler for MUSIC is 0.422m/s, the same for the ESPRIT is 0.3229m/s, the same for the GS-based method with $Q = 1$ is 0.3005m/s, the same for the GS-based method with $Q = 4$ is 0.2729m/s and the same for the GS-based method with $Q = 8$ is 0.2183m/s. Similarly, in figure 3, at the SNR value of 136dB, the RMSE of location for the MUSIC is 63.45m, the same for the ESPRIT is 62.52m, the same for the GS-based method with $Q = 1$ is 61.01m, the same for the GS-based method with $Q = 4$ is 61.03m and the same for the GS-based method with $Q = 8$ is 60.5m. As lower values of RMSE prove improved detection of target parameters, it can be stated that the Group-sparsity method performs better than both the

MUSIC and the ESPRIT algorithms, for the estimation of location and Doppler of the target vehicle. The reason is that, in this bistatic Radar scenario, the source vectors have a common support set, and this allows more accurate estimation of target parameters by using the GS method, compared to the MUSIC or the ESPRIT. Both the MUSIC and the ESPRIT algorithms are based on signal subspace techniques and consider independent sources. But when a limited number of sensors are present, like in this case with roadside Radar being used by multiple users, a sparse matrix representation makes the algorithms resilient to signal variations. Additionally, the MUSIC and ESPRIT algorithms are susceptible to noise, whereas the GS method is more robust to it. Thus, the GS-based algorithm provides improved estimation of the DOA, even in the presence of external noise. Among the tests done using the Group-sparsity method, it can be noted that the level of error reduces as the number of Q is increased. This shows that increasing the amount of data helps to attain a regularization effect, which leads to improved detection of the DOA of the target vehicle. If the amount of data is increased, a better representation of the system is obtained for understanding it.

If the number of elements of the antenna is increased, the beam of the antenna becomes narrower, leading to improved angular resolution and more accurate differentiation between closely placed targets. This will lead to better estimation of the DOA of the target vehicle, which eventually results in a lower RMSE value. To evaluate this property, simulations are done with the Group-sparsity method for $Q = 1$, with a varying number of antenna elements, and the tests are conducted for 50 iterations.

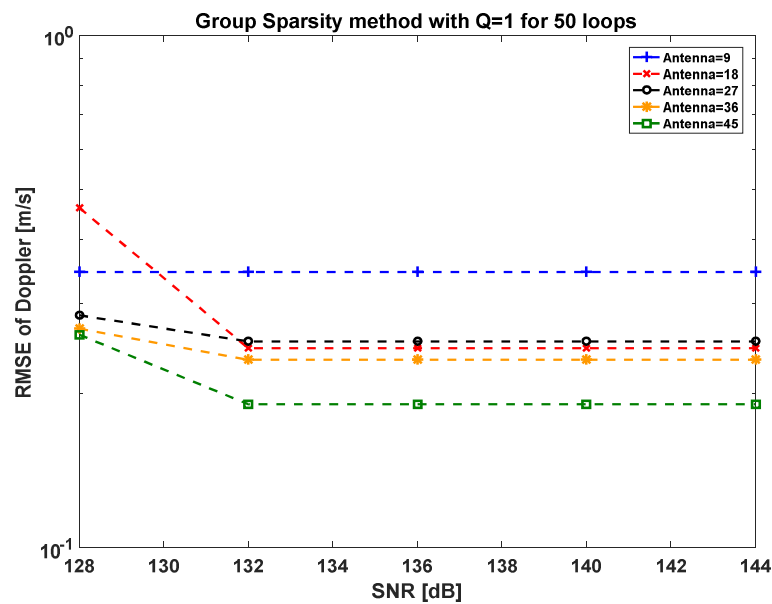


Figure 4. RMSE of Doppler v/s SNR obtained with the GS method (for $Q = 1$) while varying the number of antenna elements for 1 target.

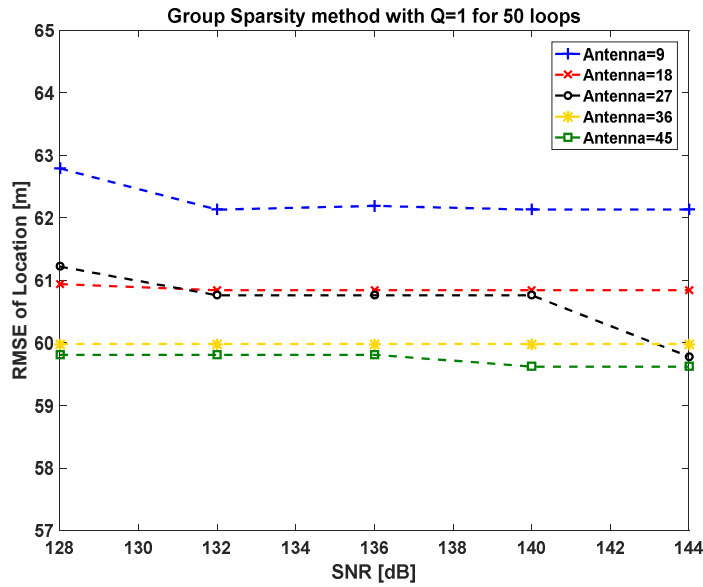


Figure 5. RMSE of location v/s SNR obtained with the GS method (for Q = 1) while varying the number of antenna elements for 1 target.

As observed from figure 4, the RMSE of the Doppler estimation is highest when the number of elements of the antenna is 9 and the value is lowest when the number of elements of the antenna is 45, for increasing values of the SNR. For example, at the SNR value of 132dB, the RMSE of Doppler for the number of antenna units of 9 is 0.3456m/s, and this value decreases corresponding to the increasing antenna size till the same value for the number of antenna units of 45 is 0.1907m/s. Similarly, in figure 5, at the SNR value of 132dB, the RMSE of location for the number of antenna units of 9 is 62.13m, this value decreases corresponding to the increasing antenna size till the same for the number of antenna units of 45 is 59.81m.

Since the error level is lowest with the GS method for Q = 8, as per figures 2 and 3, simulations are done with the GS method for Q = 8, with a varying number of antenna elements, and the tests are conducted for 50 iterations.

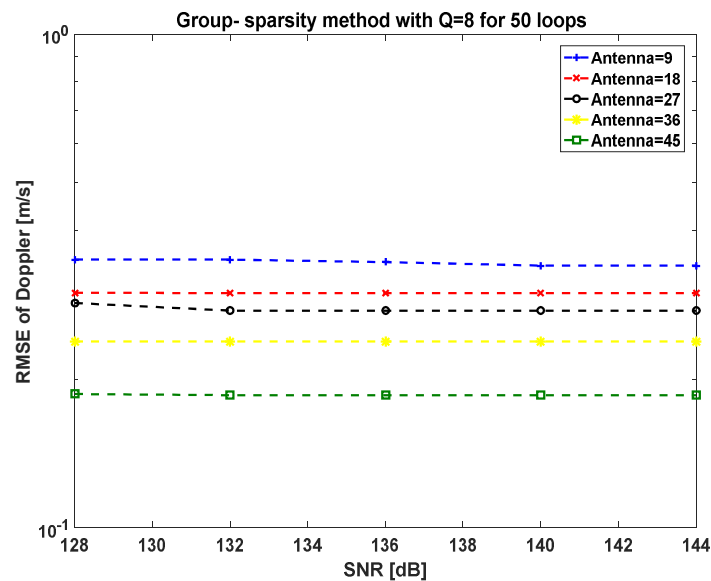


Figure 6. RMSE of Doppler v/s SNR obtained with the GS method (for Q = 8) while varying the number of antenna elements for 1 target.

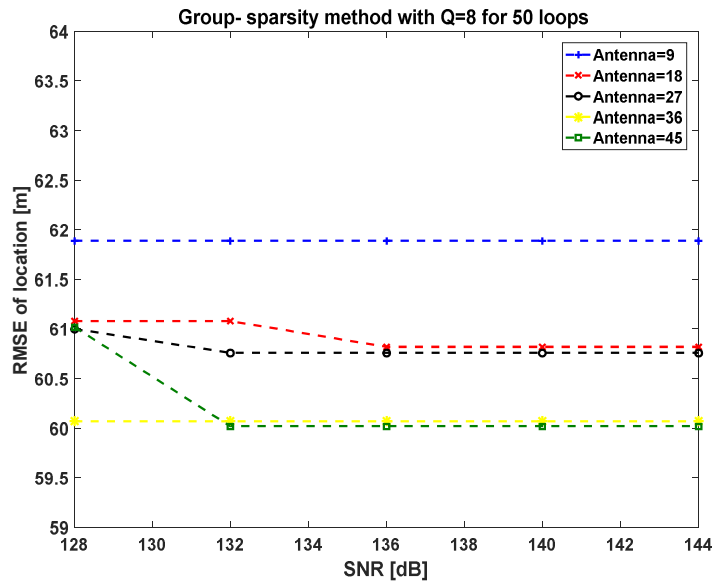


Figure 7. RMSE of location v/s SNR obtained with the GS method (for Q = 8) while varying the number of antenna elements for 1 target.

As observed from figure 6, the RMSE of the Doppler estimation is highest when the number of elements of the antenna is 9 and the value is lowest when the number of elements of the antenna is 45, for increasing values of the SNR. At the SNR value of 132dB, the RMSE of Doppler for the antenna units of 9 is 0.3496m/s; this value decreases corresponding to the increasing antenna size and the same for the antenna units of 45 is 0.1858m/s. Similarly, in figure 7, at the SNR value of 132dB, the RMSE of location for the number of antenna units of 9 is 61.89m, this value decreases corresponding to the increasing antenna size and the same for the number of antenna units of 45 is 60.02m.

The detection of the target with the highest RCS is dependent on the aspect angle, along with the shape of the vehicle. The target RCS is defined as the intensity of the backscattered energy that has the same polarization as the Radar's receiving antenna. SNR is the ratio of the desired Radar signal power to the unwanted noise signal power. A higher value of RCS means a stronger signal echo from the target, and thus, less error is present in the evaluation of location and Doppler of the particular target. To evaluate this property, simulations are done with the Group-sparsity method for $Q = 8$, while changing the RCS values to 0.1 m^2 , 1 m^2 and 10 m^2 , and the tests are conducted for 50 iterations.

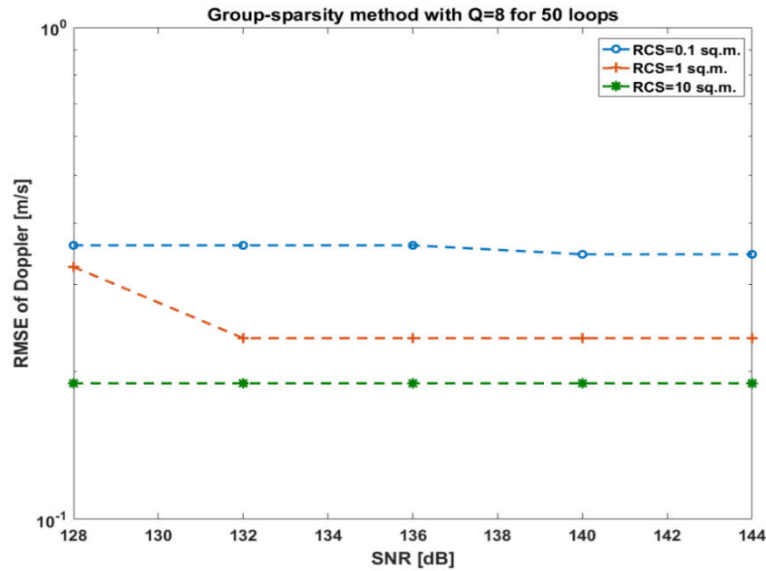


Figure 8. RMSE of Doppler v/s SNR obtained with the GS method (for Q = 8) while varying the RCS values of 1 target.

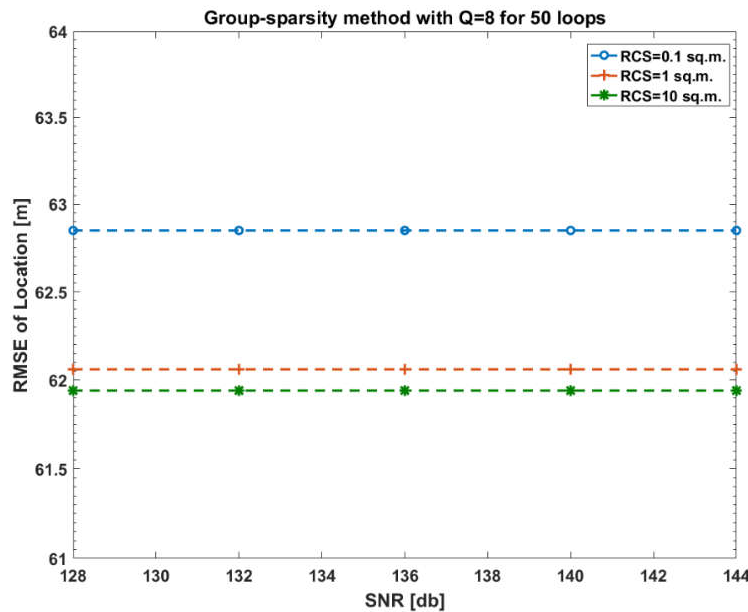


Figure 9. RMSE of location v/s SNR obtained with the GS method (for Q = 8) while varying the RCS values of 1 target.

As it is observed from figure 8, the RMSE for the Doppler estimation is highest when the RCS value is 0.1 m² and the value is lowest when the RCS value is 10 m², for increasing values of the SNR. For example, at the SNR value of 132 dB, the RMSE of Doppler for the RCS value of 0.1 m² is 0.3605m/s, the same for the RCS value of 1 m² is 0.2335m/s, and the same for the RCS value of 10 m² is 0.189m/s. Similarly, in figure 9, at the SNR value of 132dB, the RMSE of location for the RCS value of 0.1 m² is 62.85m, the same for the RCS value of 1 m² is 62.06m, and the same for the RCS value of 10 m² is 61.94m.

Conclusion

A sparse representation of the bistatic radar signal model is employed, on which the GS method, MUSIC, and ESPRIT algorithms are applied for target localization and Doppler estimation. MATLAB simulations validate the performance of these techniques, revealing that the GS method consistently outperforms MUSIC and ESPRIT in terms of estimation accuracy. Using the GS-method and by varying the quantity of processed columns of the data matrix (Q), it is further observed that this method with a higher number of columns provides the lowest level of error. To obtain additional knowledge on this, simulations were performed with the GS method while changing the number of antenna elements, once for $Q = 1$ and then for $Q = 8$. Results indicate that increasing the number of antennas enhances angular resolution and reduces error levels. Moreover, experiments with varying Radar Cross Section (RCS) values demonstrate that higher RCS—implying stronger reflected signal power—leads to lower estimation errors; for example, an RCS of 10 m^2 results in substantially lower errors compared to an RCS of 0.1 m^2 . Future work may extend this analysis to multi-target scenarios and include comparisons with other advanced algorithms such as Root-MUSIC and Compressive Sensing.

Further work can be conducted by increasing the number of targets and observing the effect on error levels. Also, tests can be conducted to compare the effectiveness of algorithms, such as Root-MUSIC and the Compressive Sensing technique.

Acknowledgments

Pallabi Biwas and Samarendra Nath Sur acknowledge administrative and technical support from Sikkim Manipal Institute of Technology, Sikkim Manipal University, Sikkim, India.

REFERENCES

- [1] Engels, F.; Heidenreich, P.; Wintermantel, M.; Stacker, L.; Kadi, M.A.; Zoubir, A.M. *Automotive Radar Signal Processing: Research Directions and Practical Challenges. IEEE Journal of Selected Topics in Signal Processing* 2021, 15, 865–878. <https://doi.org/10.1109/JSTSP.2021.3093043>.
- [2] Biswas, P; Bera, R; and Shome, S. *Integrated Radar and Communication Systems for Highly Automated Vehicles, Telecommunications and Radio Engineering, Volume 82, Issue 6, 2023, pp. 39-52, doi: 10.1615/TelecomRadEng.2023046609.*
- [3] Moussa A.; and Liu W.; *Enhanced Detection in Automotive Applications Using Bistatic Radar with Cooperative Roadside Sensors. 2021 CIE International Conference on Radar (Radar), Haikou, Hainan, China, 2021, 16494-1653. doi: 10.1109/Radar53847.2021.10028039.*
- [4] Wang, Q; Yu, D; and Zhu, Yi. *Angle-Range estimation for Bistatic FDA-MIMO Radar via Tensor Completion, Telecommunications and Radio Engineering, Volume 79, Issue 9, 2020, pp. 753-768.*
- [5] Venon, A.; Dupuis, Y.; Vasseur, P.; Merriaux, P. *Millimeter Wave FMCW RADARs for Perception, Recognition and Localization in Automotive Applications: A Survey. IEEE Transactions on Intelligent Vehicles* 2022, 7, 533–555. <https://doi.org/10.1109/TIV.2022.3168927>.
- [6] Yadav, R., Dahiya, P.K. & Mishra, R. *Comparative analysis of automotive radar sensor for collision detection and warning system. International Journal of Information Technology* 2020, 289–294. <https://doi.org/10.1007/s41870-018-0167-3>
- [7] Gamba, J. *Radar Signal Processing for Autonomous Driving; Signals and Communication Technology, Springer Nature Singapore Pte Ltd.: Singapore, 2020. https://doi.org/10.1007/978-981-15-3761-5.*
- [8] Gerstmair, M; Melzer, A; Onic, A; and Huemer, M. *On the Safe Road Toward Autonomous Driving: Phase Noise Monitoring in Radar Sensors for Functional Safety Compliance, IEEE Signal Processing Magazine, Volume 36, No. 5, pp. 60-70, 2019, doi: 10.1109/MSP.2019.2902914.*
- [9] Cho, S.; Song, H.; You, K.J.; Shin, H.C. *A New Direction-of-Arrival Estimation Method Using Automotive Radar Sensor Arrays. International Journal of Distributed Sensor Networks* 2017, 13. <https://doi.org/https://doi.org/10.1177/1550147717713628>.
- [10] Seo, J.; Lee, J.; Park, J.; Kim, H.; You, S. *Distributed Two- Dimensional MUSIC for Joint Range and Angle Estimation with Distributed FMCW MIMO Radars. Sensors* 2021, 21, 7618. <https://doi.org/10.3390/s21227618>.

- [11] Ahmad, M.; Zhang, X.; Lai, X.; Ali, F.; Shi, X. Low-Complexity 2D-DOD and 2D-DOA Estimation in Bistatic MIMO Radar Systems: A Reduced-Dimension MUSIC Algorithm Approach. *Sensors* 2024, 24, 2801. <https://doi.org/10.3390/s24092801>.
- [12] Pang, Y.; Liu, S.; He, Y. A PE-MUSIC Algorithm for Sparse Array in MIMO Radar. *Hindawi, Mathematical Problems in Engineering*, Volume 2021, Article ID 6647747, 1-7, <https://doi.org/10.1155/2021/6647747>.
- [13] Wen, D.; Yi, H.; Zhang, W.; & Xu, H. 2D-Unitary ESPRIT Based Multi-Target Joint Range and Velocity Estimation Algorithm for FMCW Radar. *Applied Sciences*, 2023, 13(18), 10448. <https://doi.org/10.3390/app131810448>
- [14] Zhang, C.; Pang, Y. Sparse Array Angle Estimation Using Reduced-Dimension ESPRIT-MUSIC in MIMO Radar, *Hindawi Publishing Corporation, The Scientific World Journal* Volume 2013, Article ID 784267, <http://dx.doi.org/10.1155/2013/784267>.
- [15] Abyshev, S; and Abysheva, E. Coupled C-ESPRIT-Based Azimuth and Elevation Angle Estimation with Minimum Variance, *Telecommunications and Radio Engineering*, Volume 83, Issue 12, 2024, pp. 43-50, doi: 10.1615/TelecomRadEng.2024053712.
- [16] Chalise, B.K. et al., Sparsity-based Distributed DoA Estimation for Radar Networks, 2022 IEEE Radar Conference (RadarConf22), New York City, NY, USA, 2022, 1-6, doi: 10.1109/RadarConf2248738.2022.9764347.
- [17] Amani, N.; Jansen, F.; Filippi, A.; Ivashina, M.V.; Maaskant, R. Sparse Automotive MIMO Radar for Super-Resolution Single Snapshot DOA Estimation With Mutual Coupling. *IEEE Access* 2021, 9, 146822–146829. <https://doi.org/10.1109/ACCESS.2021.3123456>.
- [18] Sun, S.; Zhang, Y.D. 4D Automotive Radar Sensing for Autonomous Vehicles: A Sparsity-Oriented Approach. *IEEE Journal of Selected Topics in Signal Processing* 2021, 15, 879–891. <https://doi.org/10.1109/JSTSP.2021.3093267>.
- [19] Amin, V.S.; Zhang, Y.D.; Himed, B. Group Sparsity-Based Local Multipath Doppler Difference Estimation in Over-the-Horizon Radar, 2020 IEEE International Radar Conference (RADAR), Washington, DC, USA, 2020, 436-441. doi: 10.1109/RADAR42522.2020.9114721.
- [20] Correas-Serrano, A.; González-Huici, M.A. Experimental Evaluation of Compressive Sensing for DoA Estimation in Automotive Radar. *Proceedings of the 19th International Radar Symposium (IRS)*. IEEE, 2018, 1–10. <https://doi.org/10.1109/IRS.2018.8448167>.
- [21] Elster, L; Holder, M.F.; and Rapp, M. A dataset for radar scattering characteristics of vehicles under real-world driving conditions: major findings for sensor simulation, *IEEE Sensors Journal*, Vol. 23, no. 5, pp. 4873–82, 2023.
- [22] Moussa, A.; Liu, W. A Two-Stage Sparsity-Based Method for Location and Doppler Estimation in Bistatic Automotive Radar. *Proceedings of the 2023 IEEE Statistical Signal Processing Workshop (SSP)*. IEEE, 2023, 487–491. <https://doi.org/10.1109/SSP.2023.9999999>
- [23] Moussa, A.; Liu, W.; Zhang, Y.D.; Greco, M.S. Multi-Target Location and Doppler Estimation in Multistatic Automotive Radar Applications. *IEEE Transactions on Radar Systems* 2024. <https://doi.org/10.1109/TRS.2024.1000000>.
- [24] Salem, S.G.; Hosseney, M.E. Signal processing implementation of low-cost target speed detection of CW radar using FPGA. *International Journal of Information Technology*, 16, 4565– 4572 (2024). <https://doi.org/10.1007/s41870-024-02033-3>
- [25] Ebreghed, D. Overview of Angle Estimation Algorithms in Bistatic MIMO Radar Systems, *International Journal of Engineering Innovation & Research*, Volume 9, Issue 1, 2020, 31- 44.